Taylor & Francis
Taylor & Francis Group

RESEARCH PAPER

🔓 OPEN ACCESS ◉ Check for updates

Ion channel mechanisms underlying frequency-firing patterns of the avian nucleus magnocellularis: A computational model

Ting Lu[a], Kirstie Wade[a], Hui Hong [iD][a], and Jason Tait Sanchez[a,b,c]

[a]Roxelyn and Richard Pepper Department of Communication Sciences and Disorders, Northwestern University, Evanston, IL, USA; [b]Department of Neurobiology, Northwestern University, Evanston, IL, USA; [c]The Hugh Knowles Hearing Research Center, Northwestern University, Evanston, IL, USA

ABSTRACT

We have previously shown that late-developing avian nucleus magnocellularis (NM) neurons (embryonic [E] days 19–21) fire action potentials (APs) that resembles a band-pass filter in response to sinusoidal current injections of varying frequencies. NM neurons located in the mid- to high-frequency regions of the nucleus fire preferentially at 75 Hz, but only fire a single onset AP to frequency inputs greater than 200 Hz. Surprisingly, NM neurons do not fire APs to sinusoidal inputs less than 20 Hz regardless of the strength of the current injection. In the present study we evaluated intrinsic mechanisms that prevent AP generation to low frequency inputs. We constructed a computational model to simulate the frequency-firing patterns of NM neurons based on experimental data at both room and near physiologic temperatures. The results from our model confirm that the interaction among low- and high-voltage activated potassium channels (K_{LVA} and K_{HVA}, respectively) and voltage dependent sodium channels (Na_V) give rise to the frequency-firing patterns observed in vitro. In particular, we evaluated the regulatory role of K_{LVA} during low frequency sinusoidal stimulation. The model shows that, in response to low frequency stimuli, activation of large K_{LVA} current counterbalances the slow-depolarizing current injection, likely permitting Na_V closed-state inactivation and preventing the generation of APs. When the K_{LVA} current density was reduced, the model neuron fired multiple APs per sinusoidal cycle, indicating that K_{LVA} channels regulate low frequency AP firing of NM neurons. This intrinsic property of NM neurons may assist in optimizing response to different rates of synaptic inputs.

Introduction

In the auditory system of all vertebrates, the temporal pattern of action potential (AP) firing is imperative for the encoding of behaviorally relevant spectral and temporal acoustic cues.[1-3] Fundamental to this are highly specialized anatomic and physiologic properties shared across species at the molecular, cellular and neural network level.[4,5] For example, bushy cells of the mammalian anteroventral cochlear nucleus (AVCN) and the avian analog, nucleus magnocellularis (NM) receive input from a few auditory nerve fibers through large endbulb of Held synapses.[6,7] This unique anatomic feature permits ultrafast and highly reliable synaptic transmission.[8,9] AVCN bushy cells and NM neurons have distinct physiologic features as well.[10,11] One such property is shown in Fig. 1A. Here, an individual NM neuron generates a
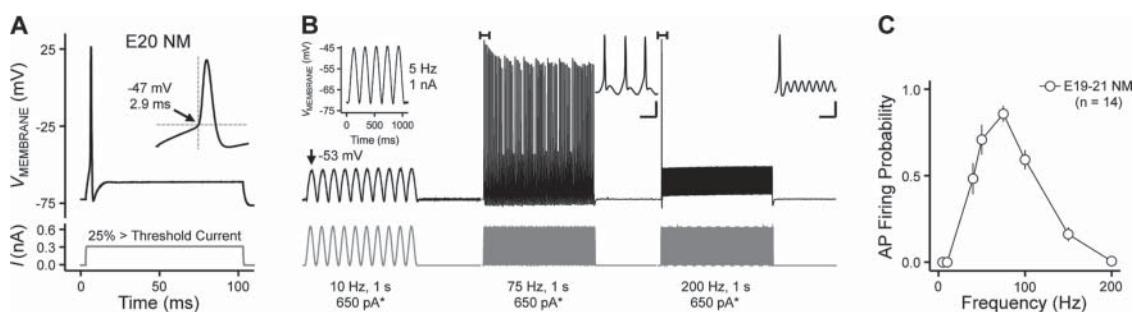
single onset AP in response to a sustained depolarizing current injection. This physiologic response property of NM neurons is sent to their bilateral target nuclei and is used to encode timing cues for sound localization.[12,13]

We have previously shown that late-developing NM neurons (embryonic [E] days 19–21) that represent the mid- to high-frequency region of the nucleus also fire unique AP patterns in response to sinusoidal current injections of varying frequencies[14] (Fig. 1B). NM neurons fire optimally at mid frequencies (75–100 Hz, Fig. 1B, *middle*) and only fire a single onset AP at higher frequencies (> 200 Hz, Fig. 1B, *right*). Interestingly, NM neurons do not generate APs in response to low frequency stimuli (< 20 Hz, Fig. 1B, *left*), regardless of the strength of the input current injection (e.g., 5 Hz and 1 nA, Fig. 1B, *left, inset*). As such, NM neurons fire

Figure 1. Mid- to high-frequency NM neurons show distinct firing patterns in response to sustained and sinusoidal current injections. (A) Representative voltage trace recorded from a late-developing NM neuron (E20) in response to sustained current injection shown below (325 pA, 100 ms). The strength of sustained current is 25% above threshold current ($I_{Threshold}$ = 260 pA). The inset marks the AP voltage threshold. In this and subsequent figures, schematic stimuli used to evoke responses are shown below representative traces. (B) Representative voltage traces in response to 5 (left, inset), 10 (left), 75 (middle), and 200 Hz (right) sinusoidal current injections recorded from the same NM neuron shown in (A). The strength of 10, 75, and 200 Hz sinusoidal current is 150% above threshold current (i.e., 650 pA*). In this and subsequent figures, * = 150% above threshold current. The arrow in the left panel points the maximum depolarizing value of the voltage response (i.e., -53 mV). In this and subsequent figures, brackets point the traces that are enlarged in the insets, insets shown with scale bar are due to space limitations, otherwise complete x and y axis are provided. Scale bar values for the insets are 25 mV/10 ms. (C) Population data (E19–21, n = 14) showing the firing probability per sinusoidal cycle, calculated as the number of APs divided by the total number of sinusoidal cycles, plotted as a function of stimulus frequency. Error bars = standard error of the mean. Data modified from Hong et al., 2016.

APs in response to sinusoidal current injections that resembles a band-pass filter (Fig. 1C, see Results).

Essential to these AP firing patterns are voltage dependent ion channels, including low- and high-voltage activated potassium (K_{LVA} and K_{HVA}, respectively) and voltage dependent sodium (Na_V) channels.[15,16] It is well documented that late-developing NM neurons have large potassium conductances mediated by K_{LVA} and K_{HVA}.[17,18] K_{LVA} channels are activated on the slight depolarization of the membrane potential and play a major role in controlling neural excitability for NM neurons.[18-20] At more positive membrane voltage, K_{LVA} channels mediate approximately 50% of the total potassium current.[14] The remaining current is dominated by K_{HVA} channels, which regulate AP repolarizing kinetics and high-frequency firing.[21,22] We hypothesized that low frequency sinusoidal stimuli (< 20 Hz) fail to elicit APs due to the activation of K_{LVA}, which repolarizes the membrane and prevents the activation of Na_V channels. We originally tested this hypothesis by experimentally blocking K_{LVA} with bath application of Dendrotoxin (DTx, 0.1 μM), a specific K_V1-containing K_{LVA} channel blocker. Blockade of K_{LVA} with DTx slightly depolarized the membrane and significantly increased neural excitability such that multiple spikes were evoked in response to a lower amount of sustained current injection (Fig. 2A). An increase in AP firing was also observed during the 10 Hz sinusoidal current injection protocol (Fig. 2B).

However, bath application of DTx during this condition resulted in a dramatic change in AP activity. The NM neuron's significant increase in excitability made the discernment of evoked versus spontaneous AP generation impossible (Fig. 2C). In addition, the real-time and dynamic interaction between K_V and Na_V channels could not be profiled experimentally, which hindered the interpretation of the results.

To better address these experimental issues, we constructed a computational model to test our hypothesis based on intrinsic properties of NM neurons and explored mechanisms underlying low frequency AP firing patterns of the avian NM. Using this model, AP frequency-firing patterns in response to low-, mid-, and high-frequency sinusoidal current injections were simulated at both room and near physiologic temperatures. Relevant contributions of K_{LVA}, K_{HVA}, and Na_V are suggested, and the importance of K_{LVA} in low frequency NM response property is evaluated.

Results

Simulating AP firing of NM neurons in response to sustained current injection

In response to a sustained depolarizing current injection, late-developing NM neurons (>E19) fire a single onset AP followed by slight and persistent membrane voltage depolarization.[10] Fig. 1A shows a representative voltage response recorded from an E20 NM
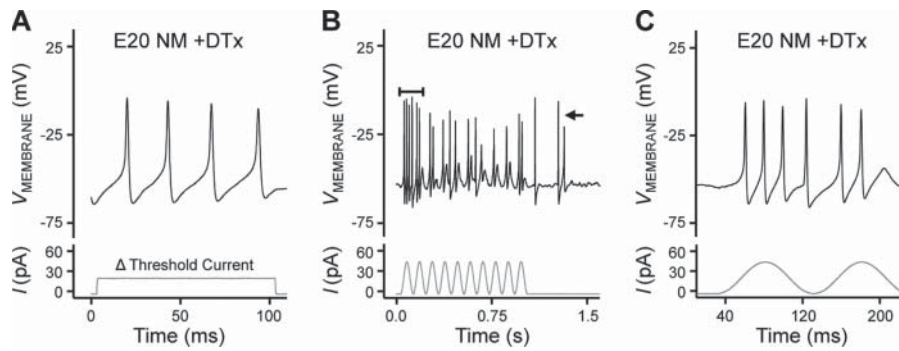
Figure 2. Application of DTx changes the firing patterns of NM neurons in response to sustained and sinusoidal current injections. (A) Representative voltage trace in response to sustained current injection (23 pA, 100 ms) during DTx (0.1 μM) application. Δ threshold current = reduction in current needed to elicit AP generation after DTx application. (B) Representative voltage trace in response to 10 Hz sinusoidal current injection (50 pA) during DTx application. The arrow marks spontaneous APs. The area indicated by the bracket is expanded and shown in (C). Traces shown in this figure were recorded from the same NM neuron shown in Fig. 1.

neuron. For this representative NM neuron, AP generation occurred 2.9 ms after the onset of the stimulus. The threshold for AP generation (i.e., the point at which the membrane voltage shifted from a passive rise to an active response) was −47 mV (Fig. 1A, inset). Blocking K_{LVA} channels with DTx resulted in multiple APs throughout the duration of a significantly smaller current injection (325 pA vs. 23 pA, Fig. 1A vs. Fig. 2A, respectively).

We first tested if our model NM neuron presented with similar AP firing phenotypes at room temperatures (25°C), the temperature at which our experimental data were obtained. Using the model NM neuron, responses for sustained current injection were simulated with parameters listed in Tables 1 and 2.

Table 1. Model Parameters.

Current (I)	Formula
I Na$_V$	
m_∞	1/(1+exp(-(v+43)/7.5))
h_∞	1/(1+exp((v+65)/6.5))
τ_m	(10/(5*exp((v+60)/18)+36*exp(-(v+60)/25))+0.04
τ_h	(100/(7*exp((v+60)/11)+10*exp(-(v+60)/25))+0.6
q10	3
T_0	22°C
I K$_{LVA}$	
w_∞	1/(1+exp(-(v+67)/8))
z_∞	1/(1+exp(-(v+71)/10))
τ_w	(100/(6*exp((v+60)/6)+16*exp(-(v+60)/45))+1.5
τ_z	(100/(exp((v+60)/20)+exp(-(v+60)/8))+50
q10	3
T_0	22°C
I K$_{HVA}$	
n_∞	1/(1+exp(-(v+35)/14))
p_∞	1/(1+exp(-(v+71)/10))
τ_n	(100/(11*exp((v+60)/24)+21*exp(-(v+60)/23))+0.7
τ_p	(100/(4*exp((v+60)/32)+5*exp(-(v+60)/22))+5
q10	3
T_0	22°C

Using a square pulse current injection of 325 pA (100 ms duration), the model NM neuron fired a single onset AP (Fig. 4A$_1$). The AP delay was 2.8 ms and its voltage threshold was −45 mV (Fig. 4A$_1$, inset), a result similar to the representative NM neuron shown in Fig. 1A. Fig. 4A$_2$ shows the activation of Na$_V$ and K$_V$ channel currents. The AP was generated when the Na$_V$ current surpassed the large transient component of the K$_V$ current (Fig. 4A$_2$, inset). The large transient K$_V$ current was consistently observed for all simulations (see Figs. 5–7). This is generally due to the fast dynamics on the membrane voltage because of the generated AP. For example, during the depolarization phase of the AP, membrane voltage increased rapidly and a large amount of K$_V$ channels were activated. As a result, I_K increased rapidly as observed at the onset of the sustained voltage step in Fig. 3, forming the rising phase of the I_K transient. During the repolarizing phase of the AP, membrane voltage decreased rapidly and K$_V$ channels deactivated. As a result, I_K decreased rapidly as observed at the offset of the voltage step in Fig. 3, forming the decay phase of the I_K transient.

Table 2. Single Compartment Model.

Variable	Parameters
Axial Resistance	50 Ωcm
Temperature	25°C/35°C
E_{Na}	30 mV
E_K	-80 mV
Length	20 μm
Diameter	20 μm
gLeak	0.0002 S/cm^2
gNa$_V$	0.04 S/cm^2
gK$_{LVA}$	0.0069 S/cm^2
gK$_{HVA}$	0.002 S/cm^2

Our modeling data, especially for the "real-time" K_V current, largely resemble experimental data previously published.[23-25] In these studies, AP waveforms were applied to neurons as voltage commands and the real-time current response was recorded (referred to as action potential clamp). With an "AP" voltage command applied to the neuron a large transient K_V current was observed, a similar result reported here. For comparison purposes in this and subsequent figures, the total outward K_V current was flipped ($-I_K$) and superimposed onto the Na_V currents.

Following the onset AP, Na_V channels inactivated and the membrane voltage repolarized for the remaining duration of the stimulus. Fig. 4A$_3$ shows the percentage of Na_V channel availability (h, gray trace) and the percentage of Na_V channels in an inactivation state ($1-h$, green trace). Throughout the duration of the sustained stimulus when Na_V channels were either unavailable or in a closed state, K_V current remained activated, counteracting the injected current and resulted in slight and persistent depolarization with no further AP generation (Fig. 4A$_{1-2}$). Due to its low voltage dependence, K_{LVA} channels activated earlier and mediated a substantially larger current than K_{HVA} channels during the stimulation (Fig. 4A$_4$, *inset*).

We next set the K_{LVA} channel density (i.e., gK_{LVA}, see Table 2) of the model NM neuron to equal zero. This simulates controlled blockade of K_{LVA} by DTx (100% blockade of K_{LVA} current). When K_{LVA} were blocked, the membrane potential slightly depolarized (-71 mV to -68 mV) and 4 APs were evoked in response to the 100 ms sustained current injection (Fig. 4B$_1$). The amount of current required to evoke AP generation from the model NM neuron was markedly smaller (325 pA vs. 50 pA). The total amount of Na_V and K_V current was also reduced (Fig. 4B$_2$). Figure 4B$_3$ shows availability and inactivation state of Na_V channels during the K_{LVA} blockade. The reduction in Na_V current and changes in availability/inactivation properties during K_{LVA} blockade was consistently observed for all simulations (see Fig. 5–7). This is largely due to the membrane voltage dependence of Na_V and K_V channels. Two primary factors contribute to the change in membrane voltage dynamics. First, there is a decrease in the strength of injected current required to reach AP generation and second, blocking K_{LVA} channels increases overall membrane voltage and excitability. As shown in Fig. 4B$_1$, the amount of current injection was 50 pA
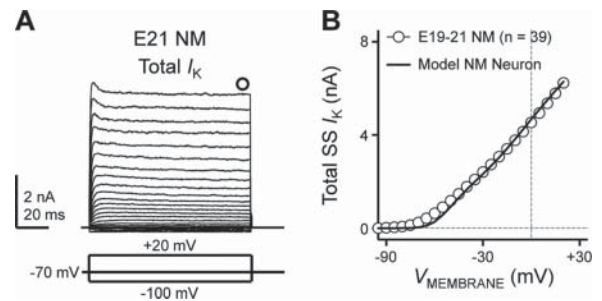

Figure 3. Current-voltage relationship of total potassium currents. (A) Representative K_V current traces (Total I_K) recorded from an NM neuron (E21) in response to membrane voltages clamped from -100 to $+20$ mV (voltage step = 5 mV, voltage duration = 100 ms). Circle at the end of current traces represent time window of measured steady-state K_V currents (Total SS I_K). (B) Total SS I_K show a nonlinear change as a function of membrane voltages for NM neurons (empty symbols, mean $\pm$ standard error of the mean, E19–21, n = 39) and for the single-compartment model (solid line). Experimental data modified from Hong et al., 2016.

(compared with 325 pA in Fig. 4A$_1$). With decreased stimulus intensity and blockade of K_{LVA}, membrane voltage dynamics changed dramatically in the simulation, leading to reduced Na_V current and changes in Na_V channel availability and inactivation properties. With 100% K_{LVA} blocked, there was no outward K_{LVA} current to counteract the depolarizing current command at low membrane voltages (Fig. 4B$_4$). As such, the membrane voltage gradually depolarized after the first AP and a subpopulation of Na_V channels recovered from inactivation, permitting the generation of subsequent APs.

Simulating AP frequency-firing patterns of NM neurons

The above results show that the model NM neuron is capable of reproducing the AP firing phenotype of late-developing NM neurons and the voltage dependence of K_{LVA} in regulating its excitability. We next tested the model neuron's ability to replicate the frequency-firing pattern of APs to sinusoidal current injections. Figure 1B shows voltage traces of a representative NM neuron in response to 5, 10, 75 and 200 Hz sinusoidal current injection. Firing probability was calculated as the average number of APs generated per sinusoidal cycle. Population data of firing probability plotted as a function of stimulus frequency is shown in Fig. 1C. This result shows that late-developing NM neurons generate APs that exhibit a band-
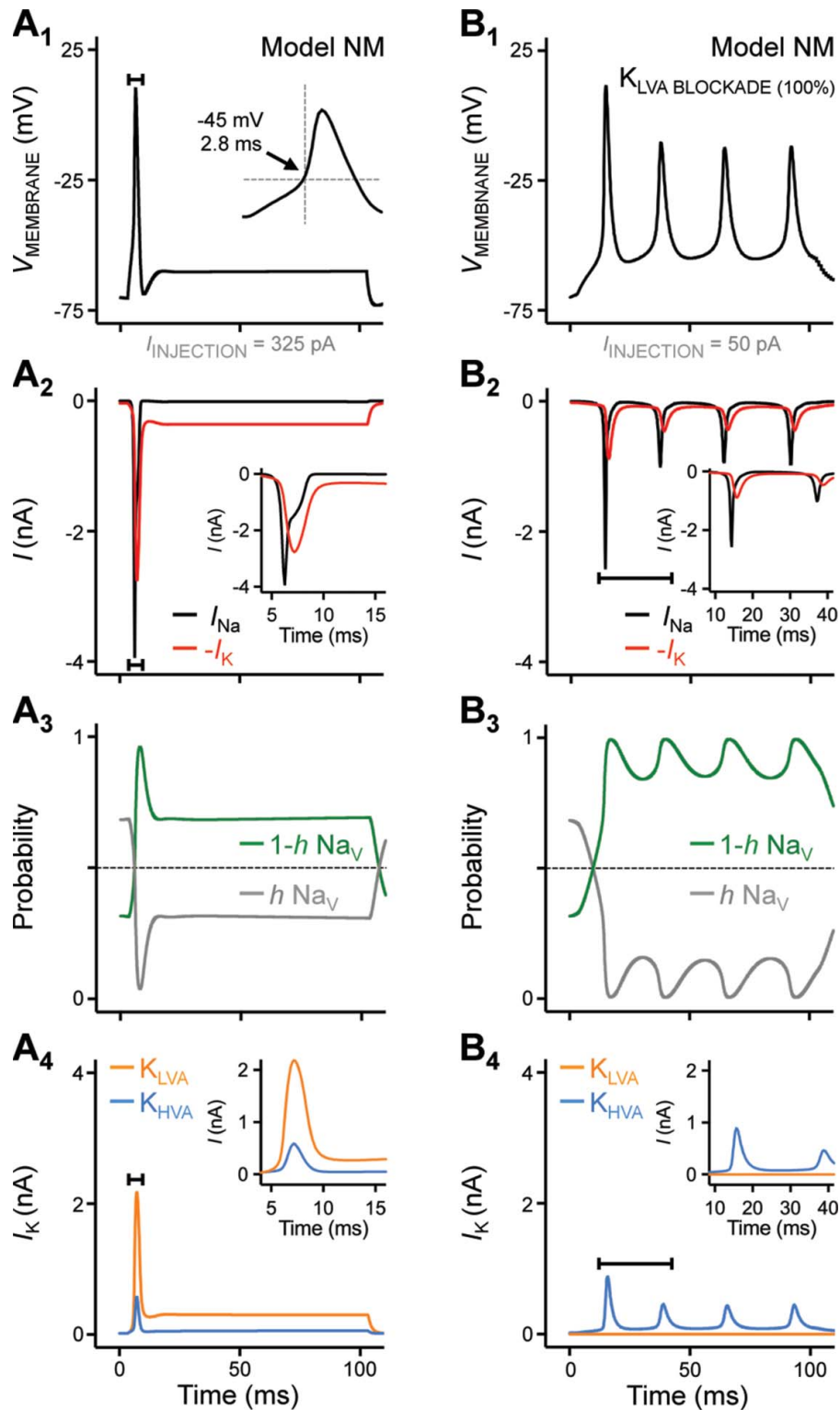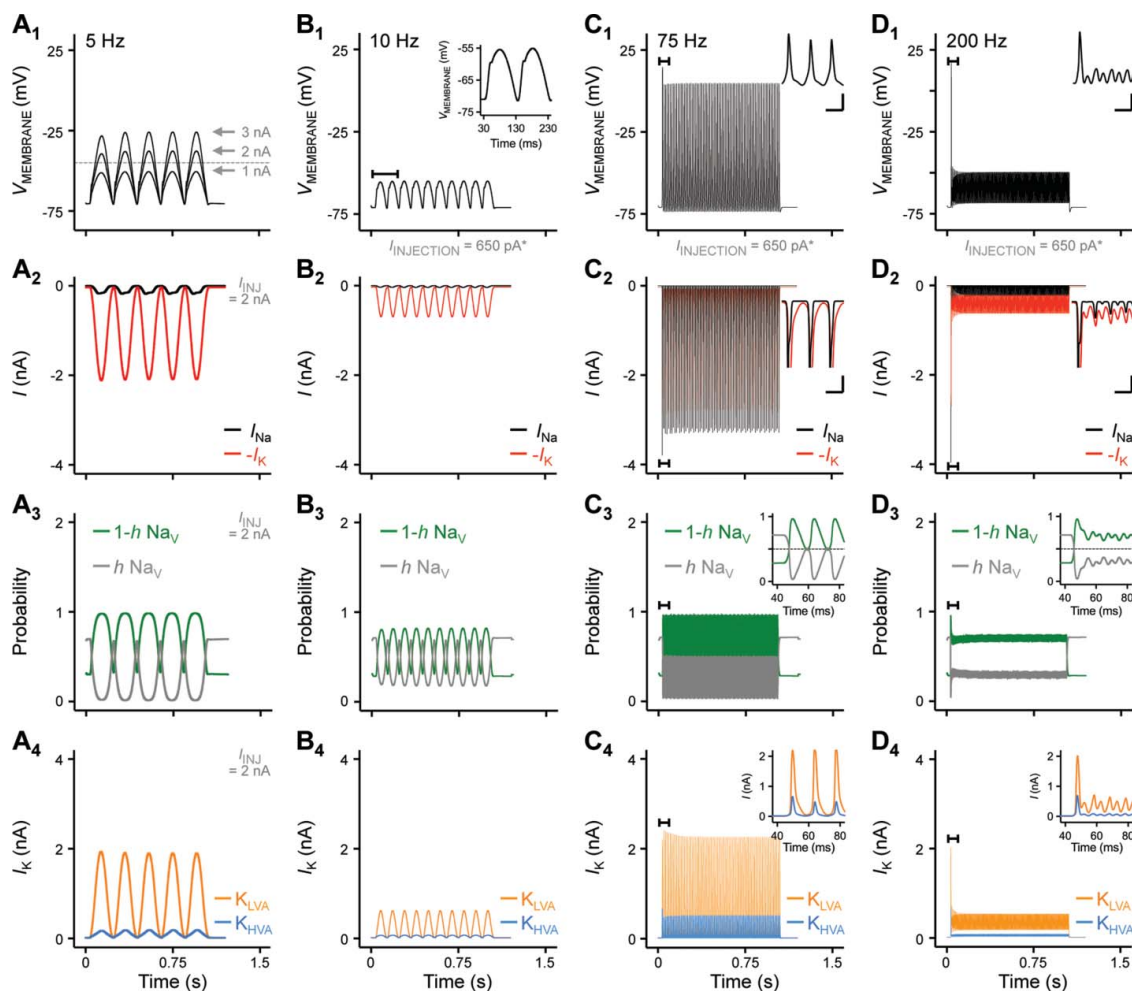
Figure 4. Simulation of NM neuron firing patterns to sustained current injection, before (A) and after (B) K_{LVA} blockade. Results were obtained from single-compartment NM model. (A_{1-4}) Responses induced by sustained current injections (325 pA, 100 ms). (B_{1-4}) Responses induced by sustained current injections (50 pA, 100 ms) with 100% K_{LVA} blockade. Traces shown are model output of membrane voltage ($V_{MEMBRANE}$, A_1 & B_1), the Na_V and K_V currents (A_2 & B_2, I_{Na} and $-I_{K}$), Na_V availability (h Na_V) and probability of inactivation state (1-h Na_V) (A_3 & B_3) and low- and high-voltage activated potassium currents (A_4 & B_4, K_{LVA} and K_{HVA}).

pass filter. They fire optimally in response to stimuli of 75 Hz and fire a single AP at the onset of the highest stimulation frequency (i.e., 200 Hz). Interestingly, NM neurons do not generate any APs at stimulus frequencies of 5 or 10 Hz. For 5 Hz stimuli, no APs can be evoked even when the stimulus intensity is significantly increased (1 nA = ~280% above threshold current, Fig. 1B *left, inset*). This is also true for responses to 10 Hz stimuli (data not shown).

Voltage responses for 5, 10, 75 and 200 Hz sinusoidal current injections were simulated using the model NM neuron (Fig. 5A$_1$-D$_1$, respectively) that closely resembled the experimental data (see Fig. 1B-C). At no time did the model NM neuron generate APs to low frequency stimulation regardless of stimulus

strength. Figure 5A$_1$ shows changes in the voltage response of the model NM neuron for a 5 Hz stimulation of increasing strengths; the extent of membrane depolarization increased with stimulus intensity. The maximum depolarizing values are -50, -42, and -32 mV for 1, 2, and 3 nA current injection, respectively. However, the threshold of AP generation was -45 mV for the model neuron using a sustained current injection of 325 pA (see Fig. 4A$_1$). Despite exceeding the threshold for AP generation with the strong current strength of 2 nA, the model NM neuron never generated an AP during the 5 Hz stimulation. This observation is due to 2 underlying ion channel mechanisms. First, the increase in the membrane voltage triggered a large outward K$_V$ current

Figure 5. Simulation of NM neuron frequency-firing patterns to sinusoidal current injections. Results were obtained from single-compartment NM model. (A$_{1-4}$ - D$_{1-4}$) Responses induced by 5, 10, 75, and 200 Hz sinusoidal current injections, respectively. Traces shown are model output of membrane voltage ($V_{MEMBRANE}$, A$_1$-D$_1$), the Na$_V$ and K$_V$ currents (A$_2$-D$_2$, I_{Na} and $-I_{Kr}$), Na$_V$ availability (h Na$_V$) and probability of inactivation state (1-h Na$_V$) (A$_3$-D$_3$) and low- and high-voltage activated potassium currents (A$_4$-D$_4$, K$_{LVA}$ and K$_{HVA}$). Scale bar values are 25 mV/10 ms and 0.5 nA/10 ms for insets in the C$_1$ & D$_1$ and C$_2$ & D$_2$, respectively.
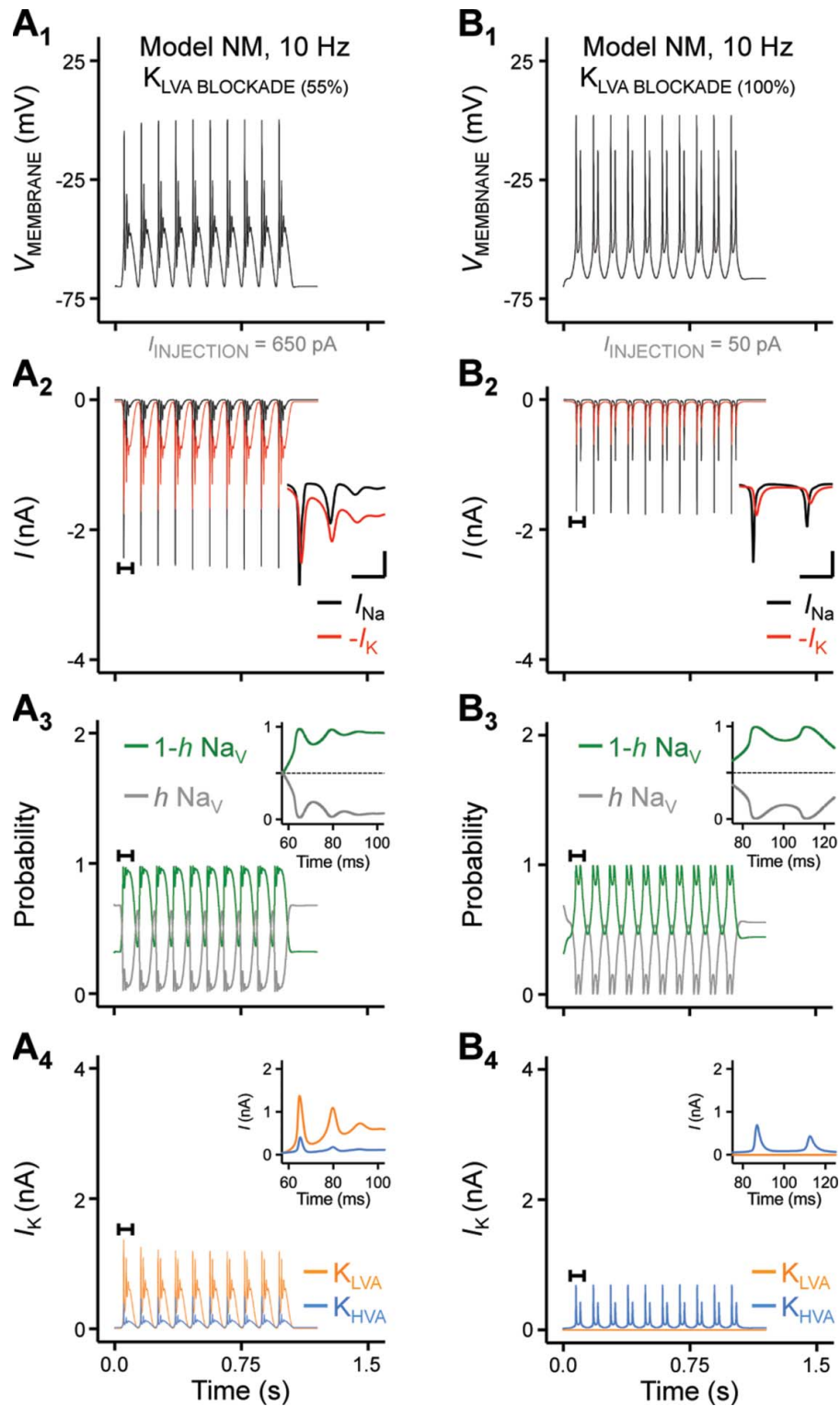
Figure 6. Simulation of the effect of K_{LVA} blockade on model NM's firing in response to 10 Hz sinusoidal current injection. (A_{1-4} & B_{1-4}) Responses induced by 10 Hz sinusoidal current injection with 55% and 100% K_{LVA} blockade, respectively. Traces shown are model output of membrane voltage ($V_{MEMBRANE}$, A_1 & B_1), the Na_V and K_V currents (A_2 & B_2, I_{Na} and $-I_K$), Na_V availability (h Na_V) and probability of inactivation state ($1-h$ Na_V) (A_3 & B_3) and low- and high-voltage activated potassium currents (A_4 & B_4, K_{LVA} and K_{HVA}). Scale bar values are 0.5 nA/20 ms for A_2 & B_2.
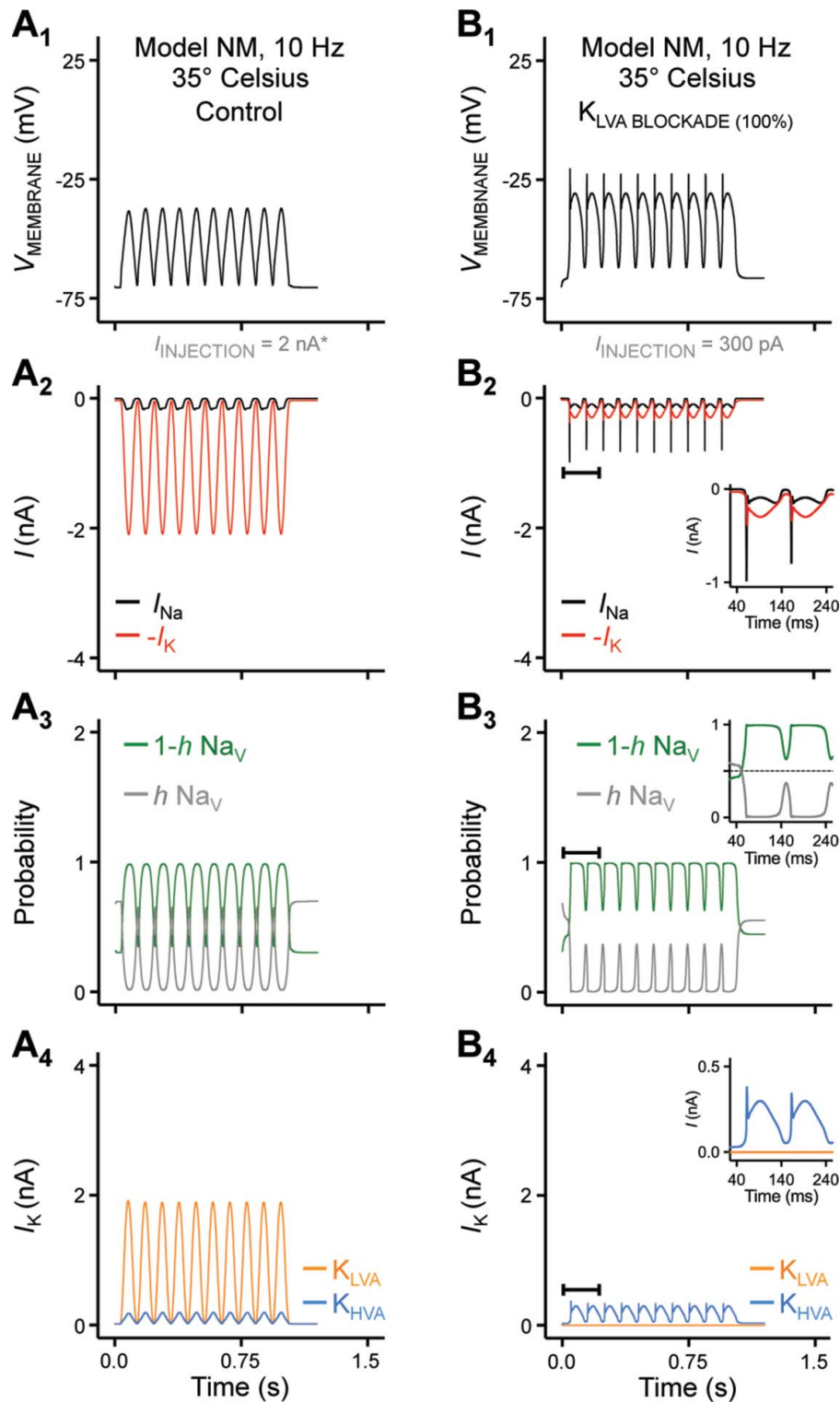
Figure 7. Simulation of the effect of temperature on model NM's firing in response to 10 Hz sinusoidal current injections under control (A) and with 100% K_LVA blockade (B). Simulations were run at near physiologic temperature of 35°C. Traces shown are model output of membrane voltage ($V_{MEMBRANE}$, A_1 & B_1), the Na_V and K_V currents (A_2 & B_2, I_{Na} and $-I_{Kr}$), Na_V availability (h Na_V) and probability of inactivation state ($1-h$ Na_V) (A_3 & B_3) and low- and high-voltage activated potassium currents (A_4 & B_4, K_LVA and K_HVA).

that strongly repolarized the membrane (Fig. 5A_2). Again, K_LVA channels mediated the largest K_V current during the stimulation (Fig. 5A_4). Second, the slow

depolarization of the membrane voltage to low frequency stimulation, along with the counteracting effect from K_LVA current, facilitated Na_V channel

closed-state inactivation and resulted in minimal Na_V current during the stimulation (Fig. $5A_{2-3}$). Additionally, the increased amount of inactivated Na_V channels likely led to a dynamic increase in AP threshold, which further prevented AP generation.

Similar results were obtained using 10 Hz stimulation. Figure $5B_1$ shows the model output induced by 10 Hz sinusoidal current injection at 650 pA (150% above the threshold current of model NM neuron). The model NM neuron did not reach the voltage threshold for AP generation (inset), because the membrane voltage was strongly repolarized by a large outward K_V current (Fig. $5B_2$). Additionally, slowly depolarized membrane voltage reduced Na_V availability and increased inactivation (Fig. $5B_3$). Similar to the 5 Hz stimulation, the total K_V current was dominated by K_{LVA} channels (Fig. $5B_4$). The important role of K_{LVA} channels in shaping firing patterns to low frequency stimulation was further tested by systematically lowering K_{LVA} conductance (see Fig. 6).

Figure $5C_1$ shows that the model NM neuron fired a single AP per cycle of a 75 Hz sinusoidal current injection (inset). This result is similar to the representative NM neuron shown in Fig. 1B for the same stimulus frequency. On the rising phase of the 75 Hz sine wave, the membrane voltage depolarized rapidly and activated a large Na_V current followed by a smaller K_V current (Fig. $5C_2$). The AP was evoked when Na_V current surpassed the K_V current (Fig. $5C_{1-2}$, insets). This result suggests that minimal closed-state Na_V inactivation occurred during mid-frequency stimulation, while the majority of Na_V channels inactivated rapidly after an AP, in contrast to that of low frequency stimulation (Fig. $5C_3$, inset). On the decay phase, the membrane voltage repolarized, K_{LVA} and K_{HVA} channels returned to resting states, and a large population of Na_V channels became available, allowing the generation of subsequent APs. The contribution to the total K_V current was dominated by K_{LVA} relative to K_{HVA} (Fig. $5C_4$, inset).

When a 200 Hz sinusoidal current was injected, the model NM neuron fired only a single onset AP at the beginning of the stimulus (Fig. $5D_1$). On the rising phase of the first sinusoidal cycle, the injected current depolarized the membrane voltage rapidly and immediately activated Na_V channels and the subsequent initial AP (Fig. $5D_{1-2}$, insets). Following the initial AP, the underlying availability and inactivation state of the Na_V channels oscillated passively with the sinusoidal injection (Fig. $5D_3$, inset). Accordingly, a relatively constant K_V current with small oscillations, which was dominated by K_{LVA} current (relative to K_{HVA} current), was observed throughout the stimulation duration (Fig. $5D_4$, inset). This constant K_V current is likely due to the incomplete deactivation of K_{LVA} channels, as a result of the short time interval between sinusoidal cycles. Therefore, the sustained activation of the K_{LVA} current prevented the activation of Na_V channels and controlled AP output for the remainder of the stimulus duration.

Effect of K_{LVA} blockade on AP low-frequency firing pattern

We hypothesized that low frequency stimuli fail to elicit APs due to the activation of K_{LVA} channels. The model NM neuron's output shows that a large K_V current is evoked during low frequency sinusoidal current injection (see Fig. $5B_1$) that is predominately mediated by K_{LVA} (see Fig. $5B_4$). We tested the effect of K_{LVA} blockade using the 10 Hz current evoked responses of the model NM neuron (Fig. 6). Reducing K_{LVA} channel density simulated the controlled blockade of K_{LVA} currents. As shown in Fig. $6A_{1-3}$, when 55% of K_{LVA} channels were blocked, APs were evoked by the 10 Hz sinusoidal stimulation set at a current strength of 650 pA and Na_V channels inactivated rapidly during AP firing. Despite 55% of K_{LVA} blockade, a significant amount of K_V current remained (Fig. $6A_2$, inset), which was dominated by the K_{LVA} channel relative to the K_{HVA} channel (Fig. $6A_4$, inset).

When 100% of K_{LVA} channels were blocked, the model NM neuron fired 2 APs per sinusoidal cycle. In addition, the amount of current required to evoke AP generation was significantly reduced to 50 pA (Fig. $6B_1$). In line with the strong blockade of K_{LVA} currents was the marked reduction in the total K_V current (Fig. $6B_2$, inset), strong Na_V inactivation induced by more depolarized membrane voltage (Fig $6B_3$, inset) as well as the complete elimination of K_{LVA} current and the larger contribution of K_{HVA} channels (Fig. $6B_4$, inset). Taken together, these results provide supporting evidence for our hypothesis that low frequency stimuli fail to elicit APs in NM neurons due to the activation of K_{LVA} channels.

Effect of temperature on NM neuron frequency-firing patterns to sinusoidal current injections

The internal body temperature for most warm-blooded animals ranges from 36°C to 39°C; birds have an average internal body temperature of ~41°C.[26] Although our simulation data was set at 25°C (to match the temperature used in the collection of experimental data) it is established that higher temperatures significantly alter the physiologic condition of NM neurons.[14,27] Whether the phenomenon and mechanisms are similar at higher temperatures is of physiologic relevance. However, it is difficult to record neuronal responses at the reported physiologic temperature of birds. This is especially true for long recording time periods across different developmental stages (as in our previous study). Taking advantage of our computational model, we next tested the effect of temperature on NM neuron frequency-firing patterns to sinusoidal current injections. Using the model NM neuron, simulations were run at a near physiologic temperature (Fig. 7). 35°C was chosen because in our previous study a subset of data was collected at this temperature to document changes in AP properties of NM.[14]

A temperature change from 25°C to 35°C increased the threshold current for AP firing of the model NM neuron, from 260 pA to 800 pA. This was consistent with our own experimental observation (data unpublished) and a previously published study in NM.[27] Therefore, the amplitude of the sinusoidal current injection was increased from 650 pA to 2 nA (i.e., 150% above AP threshold). At 35°C, the model NM neuron fired one AP per sinusoidal cycle in response to mid (75 Hz) and high frequency (200 Hz) sinusoid current injections (data not shown). The ability to maintain AP generation per cycle for a 200 Hz input is due – in part – to the dramatic improvement of AP kinetics at 35°C[14] and the increase in stimulus intensity.[27]

Despite an increase in temperature and stimulus intensity (35°C and 2 nA, respectively), no AP was evoked from the model NM neuron for a 10 Hz current injection (Fig. 7A$_1$). This was also evident for 5 Hz stimulation (data not shown) and was consistent with model data at 25°C (see Fig. 5B). The model's output of the Na$_V$ and K$_V$ currents show that the mechanism for no AP generation to low frequency input remained the same at the higher temperature

(Fig. 7A$_2$). With 10 Hz stimulation there was a large membrane depolarization (Fig. 7A$_1$) that resulted in inactivation of available Na$_V$ channels (Fig. 7A$_3$). The ratio of the total K$_V$ current was dominated by K$_{LVA}$ relative to K$_{HVA}$ (Fig. 7A$_4$).

Similar to the data at 25°C for 10 Hz stimulation, the model NM neuron fired APs when 100% of the K$_{LVA}$ channels were blocked at 35°C (Fig. 7B). Although the phenomenon and mechanisms are relatively unchanged at near physiologic temperatures, several differences were observed. First, the current injection was significantly higher due to the temperature dependent increase in threshold current (50 pA vs. 300 pA, Fig. 6B and Fig. 7B, respectively). Second, the model NM neuron fired only a single AP per sinusoidal cycle that was shorter in overall amplitude followed by strong membrane oscillation (Fig. 7B$_1$). This membrane oscillation is likely a combined result of the increased current injection, along with a higher membrane input resistance due to the blockade of K$_{LVA}$ channels. Third, the depolarized membrane oscillations resulted in dramatic changes in Na$_V$ channel availability and inactivation properties, which are partially responsible for the single and shorter AP per sinusoidal cycle during the stimulus (Fig. 7B$_{2-3}$). The shorter AP is a common feature when recorded at high temperatures in the avian auditory brainstem.[16,28] Finally, at 35°C the activation of K$_{HVA}$ channels followed the waveform of APs and membrane oscillations, with the peak amplitude slightly smaller than that at 25°C (Fig. 7B$_4$ compared with 6B$_4$). This is likely due to the small APs and membrane oscillations that only reach the threshold voltage of these channels' activation range,[14] unlike larger APs generated at 25°C.

Taken together, these results provide supporting evidence for our hypothesis that low frequency stimuli fail to elicit APs in NM neurons due to the activation of K$_{LVA}$ channels at both room and near physiologic temperatures.

Discussion

Simulation studies using our model NM neuron reproduced the frequency-firing patterns recorded experimentally at both room and near physiologic temperatures; NM neurons act as a band-pass filter to varying frequencies of sinusoidal current injections. The results from the model NM neuron confirm the

involvement of K_{LVA}, K_{HVA}, and Na_V channels that interact with each other to give rise to the AP firing patterns at low-, mid-, and high-frequency inputs. Upon low frequency sinusoidal stimulation (< 20 Hz), the membrane voltage depolarized slowly and activated a large number of K_{LVA} channels. When the K_{LVA} channel density was reduced or blocked, the model NM neuron fired multiple APs per sinusoidal cycle during low frequency stimulation protocols, confirming that low frequency stimuli fail to elicit APs in NM neurons due to the strong activation of K_{LVA} channels. This is accomplished primarily by 2 mechanisms. First, the relatively fast time course of K_{LVA} activation shunts slow membrane depolarization caused by low frequency sinusoidal current injections and second, the prolonged membrane depolarization changes AP threshold by Na_V channel inactivation.[8]

K_{LVA} channels regulate frequency-firing patterns of NM neurons to sinusoidal current injections

Our previous experimental data showed that mid- to high-frequency NM neurons are band-pass filters in response to sinusoidal current injections.[14] The relevant finding to the current study is that mid- to high-frequency NM neurons do not respond to low frequency stimuli (i.e., 5 and 10 Hz) regardless of the strength of the current injection. This suggests that NM neurons are tuned to fire APs at a very specific rate of afferent input. In the current study, our computational model provides evidence that the expression of K_{LVA} channels regulate the non-responsiveness of NM neurons to low frequency stimuli. When K_{LVA} current density was lowered, we observed multiple APs in response to each cycle of 5 and 10 Hz sinusoidal current injections. K_{LVA} channels are able to activate in an extremely fast manner.[20] In contrast, it takes relatively longer time to reach Na_V channel activation threshold during 5 and 10 Hz current injections, because of the slow changes in the membrane voltage induced by low frequency current injections. In addition, the slow-depolarizing membrane voltage, as a result of low frequency current injection and the counteracting effect from K_{LVA} channels, likely facilitates the closed-state inactivation of Na_V channels, which further prevents AP generation. This is in agreement with observation made by Oline et al., 2016 and suggests that mid- to high-frequency NM neurons reject slow depolarizing input more strongly than low-

frequency NM neurons.[8] This is likely regulated by the known tonotopic gradient of K_{LVA} distribution pattern, more specifically, K_V1-containing channels. Previous study shows that the level of $K_V1.1$ mRNA staining reduces with the decrease in frequency along the tonotopic axis of NM.[29]

In addition to our observations using the computational model, there is additional experimental evidence supporting the idea that K_{LVA} channels are important regulators of AP frequency-firing patterns. One comes from the mid- to high-frequency NM neurons during early development (E10–12). At this age range, NM neurons are low-pass filters and fire preferentially to 5 and 10 Hz sinusoidal current injections. Interestingly, K_{LVA} channels are also underdeveloped at E10–12 and their conductance accounts for only ~20% of the total K_V current.[14] The other evidence comes from the tonotopically arranged low-frequency NM neurons that are located at the most caudolateral region of the nucleus.[30] Surprisingly, these neurons at E19–21 act as low-pass filters instead of band-pass filters, and they have significantly lower amount of K_{LVA} conductances compared with that of their mid- to high-frequency counterparts (unpublished observation). This result is consistent with the aforementioned immunochemical data of $K_V1.1$ mRNA tonotopic arrangement.[29] To summarize our computational and experimental data, the amount of K_{LVA} conductances, which are age- and neuronal-type specific, shapes the frequency-firing patterns of NM neurons.

Functional significance of K_{LVA} channels during development

Our previous study shows that mid- to high-frequency NM neurons are low-pass filters early in development (E10–12) and change to band-pass filters before hatch (E19–21).[14] During the transition period at E14–16, NM neurons possess the frequency-firing pattern with some properties observed from both age groups.[14] This transition of frequency-firing patterns during development is in parallel with the gradual increase in the amount of K_{LVA} conductances – as well as – the inputs these neurons receive from the auditory nerve. At E10–12, the peripheral end organ of hearing known as the cochlea is unresponsive to sound but generates very low-frequency spontaneous AP activity that is sent to NM via the auditory nerve.[31] During

development, this low-frequency spontaneous firing is gradually replaced by tonic spontaneous AP firing at higher frequencies, along with the evoked activity by external sound that first appears around E14.[32,33] Interestingly, NM neurons also change from preferring low frequency sinusoidal current injections (i.e., 5 and 10 Hz) to stimuli with higher frequencies (i.e., > 75 Hz) during this same developmental time period.

As discussed above, K_{LVA} channels regulate this transition in frequency-firing patterns. There are 2 possible mechanisms underlying the development of K_{LVA} channels and frequency-firing patterns. First, NM neurons are genetically programmed to accommodate changing inputs from the auditory nerve.[34] Second, the cochlea and the auditory nerve have neurotrophic effect on NM neurons that results in accommodating changing rates of synaptic inputs.[34,35] We speculate that either mechanism delays the expression of K_{LVA} channels early in development, permitting NM neurons to respond to low frequency bouts of spontaneous AP activity before hearing onset (i.e., E10–12). With development and the onset of hearing (i.e., E14–16), changes in synaptic input, increases in the rate of spontaneous/evoked AP activity and upregulation of K_{LVA} channels shift NM neurons firing preferences to higher frequencies. This is further supported by the observation that the expression pattern of K_{LVA} channels is largest for mid- to high-frequency NM neurons.[29]

During post-hearing development, the cochlea also undergoes a change in its responsiveness to different sound frequencies along basilar membrane, that is, a shift in its place code properties.[36] When hearing onset just begins, the basal end of basilar membrane is the first place responsive to acoustic energy, but only to low frequency sounds. With development, the lower end of the characteristic frequencies progresses toward the apex of basilar membrane when more and more hair cells begin to become responsive to sound. It is suggested that individual neurons along the ascending auditory pathway also go through a shift in their characteristic frequencies from low to high during a critical period of hearing development.[36] Interestingly, from E14 to E21, the transition of NM frequency firing patterns to sinusoidal current injections is similar with this aforementioned shift in frequency place code processing. Therefore, our computational model in the current study proposes a potential molecular mechanism that is partially dependent on the

expression pattern of K_{LVA} channels that may contribute to the developmental shift in place code in the avian NM. Future experimental and computational studies could address this issue.

Methods

Model description

A single-compartment computational model was constructed using NEURON 7.1 (Table 1). This model contains currents mediated by K_{LVA}, K_{HVA}, Na_V, and passive leak channels. Biophysical properties of the neuron membrane are spatially uniform. Equations for these channels were based on previous publications[27,37,38] (Table 2). Parameters of K_{LVA} and K_{HVA} were adjusted such that the current-voltage curve of the model replicated that of the experimental data recorded from E19–21 NM neurons (Fig. 3). Parameters of Na_V were adjusted such that spike threshold and amplitude were similar between the model and the experimental data. Reducing the K_{LVA} channel density simulated controlled blockade of K_{LVA} channels.

For results shown in Figs 1–6, the operating temperature of the model NM neuron was 25°C, the temperature at which most of the experimental data was recorded. For results shown in Fig. 7, the operating temperature of the model was increased to 35°C to consider the behavior of the model NM neuron near physiologic temperature.

In vitro *electrophysiology in brainstem slices*

Slice preparation. Acute brainstem slices were prepared from chicken embryos from E19–21, as described previously.[39-41] Briefly, the brainstem was dissected and isolated in oxygenated low-Ca^{2+} high-Mg^{2+} modified ACSF containing the following (in mM): 130 NaCl, 2.5 KCl, 1.25 NaH_2PO_4, 26 $NaHCO_3$, 3 $MgCl_2$, 1 $CaCl_2$, and 10 glucose. ACSF was continuously bubbled throughout the experiments with a mixture of 95% O_2 / 5% CO_2 (pH 7.4, osmolarity 295–310 mOsm/l). The brainstem was blocked coronally, affixed to the stage of a vibratome slicing chamber (Ted Pella, Inc., Redding, CA) and submerged in ACSF. Bilaterally symmetric coronal slices were made (200 μm thick), and approximately 7 slices containing NM were taken from caudal to rostral, roughly representing the low-to-high frequency

regions, respectively. All neurons reported here were obtained from the rostral one-half of the entire nucleus, roughly representing the mid-to-high frequency regions of NM.

Slices were collected in a custom holding chamber and allowed to equilibrate for 1 hour at $\sim$22°C in normal ACSF containing the following (in mM): 130 NaCl, 2.5 KCl, 1.25 NaH_2PO_4, 26 $NaHCO_3$, 1 $MgCl_2$, 3 $CaCl_2$, and 10 glucose. Normal ACSF was continuously bubbled with a mixture of 95% O_2 / 5% CO_2 (pH 7.4, osmolarity 295–310 mOsm/l). Slices were transferred to a recording chamber mounted on an Olympus BX51W1 (Center Valley, PA) microscope for electrophysiological experiments. The microscope was equipped with a CCD camera, 60x water-immersion objective and infrared differential interference contrast optics. The recording chamber was superfused continuously (Welco, Tokyo, Japan) at room temperature (monitored continuously at $\sim$22–25°C, Warner Instruments, Hamden, CT) in normal oxygenated ACSF at a rate of 1.5–2 ml/min.

Whole cell electrophysiology. Current-clamp and voltage-clamp experiments were performed using an Axon Multiclamp 700B amplifier (Molecular Devices, Silicon Valley, CA). Patch pipettes were pulled to a tip diameter of 1–2 μm using a P-97 flaming/brown micropipette puller (Sutter Instrument, Novato, CA) and had resistances ranging from 3 to 6 MΩ. The internal solution of patch pipettes for recording action potentials (APs) and isolated K_V currents was potassium-based and contained the following (in mM): 105 K-gluconate, 35 KCl, 1$MgCl_2$, 10 HEPES-K^+, 5 EGTA, 44-ATP-Mg^{2+}, and 0.3 4-Tris2GTP, pH adjusted to 7.3–7.4 with KOH. Isolated K_V currents were recorded in the presence of the Na_V channel blocker tetrodotoxin (TTx, 1 μM). The junction potential was $\sim$-10 mV and was not corrected for current-clamp data reported in this study. In contrast, the voltage-clamp data of isolated K_V currents were corrected for this junction potential (Fig. 3).

Pipettes were visually guided to NM, where neurons were identified and distinguished from surrounding tissue based on cell morphology, known structure, and location of the nucleus within the slice. After a GΩ seal was attained, membrane patches were ruptured and neurons were first held in the voltage clamp mode of whole-cell configuration. A small hyperpolarizing (-1 mV, 30 ms) voltage command was presented to monitor whole-cell parameters (i.e., cell membrane capacitance, series resistance and input resistance). NM neurons were included in the data analysis only if they had series resistances < 15 MΩ. Afterwards we stayed in the voltage clamp mode for recording K_V currents or switched to current clamp mode at I = 0 for recording APs. Raw data was low-pass filtered at 2 kHz and digitized at 20 kHz using a Digidata 1440A (Molecular Devices).

All experiments were conducted in the presence of a $GABA_A$-R antagonist picrotoxin (PTX, 100 μM). Synaptic glutamate transmission was continuously blocked using DL-2-amino-5-phosphonopentanoic acid (DL-APV, 100 μM, an NMDA-R receptor antagonist) and 6-Cyano-7-nitroquinoxaline-2, 3-dione (CNQX, 20 μM, an AMPA-R receptor antagonist). AP properties were recorded and characterized by using different current-clamp protocols. AP threshold current is defined as the minimum amount of current required for neurons to generate an AP $\sim$50% of the time across 30 repetitive stimulations (interpulse stimulus intervals = 2 s). Once AP threshold current was obtained, a sustained current command (duration = 100 ms) was injected into the soma at 25% above the measured threshold current for each neuron. APs evoked by this current command were used to characterize AP properties. Each AP property was measured and averaged over 30 repetitive trials. Frequency-firing pattern of NM was obtained by injecting suprathreshold sinusoidal currents at frequency of 5, 10, 40, 50, 75, 100, 150 and 200 Hz. The strength of injected sinusoidal currents was 150% above AP threshold current for each NM neuron, to ensure robust AP generation across trials. Firing probability was calculated as the average number of APs generated per sinusoidal cycle and plotted as a function of stimulation frequency (Fig. 1C). In a subset of experiments when injecting low-frequency sinusoidal currents (i.e., < 20 Hz), we systematically increased the current strength beyond 150%, and up to nearly 1000% above AP threshold current.

Data analysis. Recording protocols were written and run using Clampex acquisition and Clampfit analysis software (version 10.3; Molecular Devices, Silicon Valley, CA). Statistical analyses and graphing protocols were performed using Prism (GraphPad versions 7.0b) and MATLAB (version R2014b; The Math Works, Natick, MA) software.

Reagents. All bath applied drugs were allowed to perfuse through the recording chamber for $\sim$10 minutes

before subsequent recordings. DL-APV, CNQX and all other salts and chemicals were obtained from Sigma-Aldrich (St. Louis, MO). PTX were obtained from Tocris (Ellisville, MO). TTx and DTx were obtained from Alomone Labs (Jerusalem, Israel).

Disclosure of potential conflicts of interest

No potential conflicts of interest were disclosed.

ORCID

Hui Hong http://orcid.org/0000-0002-2963-3771

References

[1] Suta D, Popelar J, Syka J. Coding of communication calls in the subcortical and cortical structures of the auditory system. Physiol Res 2008; 57 Suppl 3:S149-159; PMID:18481905

[2] Velluti RA, Pedemonte M. In vivo approach to the cellular mechanisms for sensory processing in sleep and wakefulness. Cell Mol Neurobiol 2002; 22:501-16; PMID:12585677; https://doi.org/10.1023/A:1021956401616

[3] Wenstrup JJ, Nataraj K, Sanchez JT. Mechanisms of spectral and temporal integration in the mustached bat inferior colliculus. Frontiers Neural Circuits 2012; 6:75; PMID:23109917; https://doi.org/10.3389/fncir.2012.00075

[4] Carr CE, Soares D. Evolutionary convergence and shared computational principles in the auditory system. Brain Behavior Evolution 2002; 59:294-311; https://doi.org/10.1159/000063565

[5] Carr CE, Soares D, Parameshwaran S, Perney T. Evolution and development of time coding systems. Curr Opinion Neurobiol 2001; 11:727-33; PMID:11741025; https://doi.org/10.1016/S0959-4388(01)00276-8

[6] Koppl C. Auditory nerve terminals in the cochlear nucleus magnocellularis: differences between low and high frequencies. J Comparative Neurol 1994; 339:438-46; PMID:8132870; https://doi.org/10.1002/cne.903390310

[7] Ryugo DK, Montey KL, Wright AL, Bennett ML, Pongstaporn T. Postnatal development of a large auditory nerve terminal: the endbulb of Held in cats. Hearing Res 2006; 216-217:100-15; https://doi.org/10.1016/j.heares.2006.01.007

[8] Oline SN, Ashida G, Burger RM. Tonotopic optimization for temporal processing in the cochlear nucleus. J Neurosci 2016; 36:8500-15; PMID:27511020; https://doi.org/10.1523/JNEUROSCI.4449-15.2016

[9] Lu T, Trussell LO. Development and elimination of endbulb synapses in the chick cochlear nucleus. J Neurosci 2007; 27:808-17; PMID:17251420; https://doi.org/10.1523/JNEUROSCI.1877-07.2007 10.1523/JNEUROSCI.4871-06.2007 10.1523/JNEUROSCI.2513-07.2007

[10] Reyes AD, Rubel EW, Spain WJ. Membrane properties underlying the firing of neurons in the avian cochlear nucleus. J Neurosci 1994; 14:5352-64; PMID:8083740

[11] Oertel D. Synaptic responses and electrical properties of cells in brain slices of the mouse anteroventral cochlear nucleus. J Neurosci 1983; 3:2043-53; PMID:6619923

[12] Koppl C. Auditory neuroscience: how to encode microsecond differences. Curr Biol 2012; 22:R56-58; PMID:22280909; https://doi.org/10.1016/j.cub.2011.11.042 10.1016/j.cub.2011.12.023

[13] Carr CE, Boudreau RE. Organization of the nucleus magnocellularis and the nucleus laminaris in the barn owl: encoding and measuring interaural time differences. J Comparative Neurol 1993; 334:337-55; PMID:8376623; https://doi.org/10.1002/cne.903340302

[14] Hong H, Rollman L, Feinstein B, Sanchez JT. Developmental profile of ion channel specializations in the Avian nucleus Magnocellularis. Front Cell Neurosci 2016; 10:80; PMID:27065805; https://doi.org/10.3389/fncel.2016.00080 10.3389/fncel.2016.00232

[15] Brown MR, Kaczmarek LK. Potassium channel modulation and auditory processing. Hearing Res 2011; 279:2-42; https://doi.org/10.1016/j.heares.2011.03.004

[16] Kuba, H, Ohmori, H. Roles of axonal sodium channels in precise auditory time coding at nucleus magnocellularis of the chick. J Physiol 2009; 587:87-100; PMID:19001045; https://doi.org/10.1113/jphysiol.2008.162651

[17] Bortone DS, Mitchell K, Manis PB. Developmental time course of potassium channel expression in the rat cochlear nucleus. Hearing Research 2006; 211:114-125; PMID:16337757; https://doi.org/10.1016/j.heares.2005.10.012

[18] Rathouz M, Trussell L. Characterization of outward currents in neurons of the avian nucleus magnocellularis. J Neurophysiol 1998; 80:2824-35; PMID:9862887

[19] Howard MA, Burger RM, Rubel EW. A developmental switch to GABAergic inhibition dependent on increases in Kv1-type K+ currents. J Neurosci 2007; 27:2112-23PMID:17314306; https://doi.org/10.1523/JNEUROSCI.5266-06.2007

[20] Johnston J, Forsythe ID, Kopp-Scheinpflug C. Going native: voltage-gated potassium channels controlling neuronal excitability. J Physiol 2010; 588:3187-200; PMID:20519310; https://doi.org/10.1113/jphysiol.2010.191973

[21] Klug A, Trussell LO. Activation and deactivation of voltage-dependent K+ channels during synaptically driven action potentials in the MNTB. J Neurophysiol 2006; 96:1547-55; PMID:16775198; https://doi.org/10.1152/jn.01381.2005

[22] Wang LY, Gan L, Forsythe ID, Kaczmarek LK. Contribution of the Kv3.1 potassium channel to high-frequency firing in mouse auditory neurones. J Physiol 1998; 509(Pt 1):183-94; PMID:9547392; https://doi.org/10.1111/j.1469-7793.1998.183bo.x

[23] Raman IM, Bean BP. Ionic currents underlying spontaneous action potentials in isolated cerebellar Purkinje neurons. J Neurosci 1999; 19:1663-74; PMID:10024353

[24] Liu PW, Bean BP. Kv2 channel regulation of action potential repolarization and firing patterns in superior cervical ganglion neurons and hippocampal CA1 pyramidal neurons. J Neurosci 2014; 34:4991-5002; PMID:24695716; https://doi.org/10.1523/JNEUROSCI.2566-13.2014 10.1523/JNEUROSCI.1690-14.2014 10.1523/JNEUROSCI.1925-13.2014 10.1523/JNEUROSCI.3541-13.2014 10.1523/JNEUROSCI.1348-14.2014 10.1523/JNEUROSCI.0999-14.2014 10.1523/JNEUROSCI.2752-13.2014 10.1523/JNEUROSCI.0538-14.2014 10.1523/JNEUROSCI.3547-13.2014

[25] Kimm T, Khaliq ZM, Bean BP. Differential regulation of action potential shape and Burst-Frequency Firing by BK and Kv2 channels in Substantia Nigra Dopaminergic Neurons. J Neurosci 2015; 35:16404-17; PMID:26674866; https://doi.org/10.1523/JNEUROSCI.5291-14.2015

[26] Bolzani R, Ruggeri F, Olivo OM. Average normal temperature of the chicken in the morning and after 1-2 days of fasting. Boll Soc Ital Biol Sper 1979; 55:1618-22; PMID:576010

[27] Howard MA, Rubel EW. Dynamic spike thresholds during synaptic integration preserve and enhance temporal response properties in the avian cochlear nucleus. J Neurosci 2010; 30:12063-74; PMID:20826669; https://doi.org/10.1523/JNEUROSCI.1840-10.2010

[28] Kuba H, Adachi R, Ohmori H. Activity-dependent and activity-independent development of the axon initial segment. J Neurosci 2014; 34:3443-53; PMID:24573300; https://doi.org/10.1523/JNEUROSCI.4357-13.2014

[29] Fukui I, Ohmori H. Tonotopic gradients of membrane and synaptic properties for neurons of the chicken nucleus magnocellularis. J Neurosci 2004; 24:7514-23; PMID:15329398; https://doi.org/10.1523/JNEUROSCI.0566-04.2004

[30] Rubel EW, Parks TN. Organization and development of brain stem auditory nuclei of the chicken: tonotopic organization of n. magnocellularis and n. laminaris. J Comparative Neurol 1975; 164:411-33; PMID:1206127; https://doi.org/10.1002/cne.901640403

[31] Jones TA, Jones SM. Spontaneous activity in the statoacoustic ganglion of the chicken embryo. J Neurophysiol 2000; 83:1452-68; PMID:10712472

[32] Jones TA, Jones SM, Paggett KC. Primordial rhythmic bursting in embryonic cochlear ganglion cells. J Neurosci 2001; 21:8129-35; PMID:11588185

[33] Jones TA, Jones SM, Paggett KC. Emergence of hearing in the chicken embryo. J Neurophysiol 2006; 96:128-41; PMID:16598067; https://doi.org/10.1152/jn.00599.2005 10.1152/jn.00537.2006

[34] Wang HC, Bergles DE. Spontaneous activity in the developing auditory system. Cell Tissue Res 2015; 361:65-75; PMID:25296716; https://doi.org/10.1007/s00441-014-2007-5

[35] Born DE, Rubel EW. Afferent influences on brain stem auditory nuclei of the chicken: presynaptic action potentials regulate protein synthesis in nucleus magnocellularis neurons. J Neurosci 1988; 8:901-19; PMID:3346728

[36] Lippe W, Rubel EW. Ontogeny of tonotopic organization of brain stem auditory nuclei in the chicken: implications for development of the place principle. J Comparative Neurol 1985; 237:273-89; PMID:4031125; https://doi.org/10.1002/cne.902370211

[37] Rothman JS, Young ED, Manis PB. Convergence of auditory nerve fibers onto bushy cells in the ventral cochlear nucleus: implications of a computational model. J Neurophysiol 1993; 70:2562-83; PMID:8120599

[38] Rothman JS, Manis PB. The roles potassium currents play in regulating the electrical activity of ventral cochlear nucleus neurons. J Neurophysiol 2003; 89:3097-113; PMID:12783953; https://doi.org/10.1152/jn.00127.2002 10.1152/jn.00126.2002 10.1152/jn.00125.2002

[39] Sanchez JT, Seidl AH, Rubel EW, Barria A. Control of neuronal excitability by NMDA-type glutamate receptors in early developing binaural auditory neurons. J Physiol 2012; 590:4801-18; PMID:22826130; https://doi.org/10.1113/jphysiol.2012.228734

[40] Sanchez JT, Wang Y, Rubel EW, Barria A. Development of glutamatergic synaptic transmission in binaural auditory neurons. J Neurophysiol 2010; 104:1774-89; PMID:20668278; https://doi.org/10.1152/jn.00468.2010

[41] Sanchez JT, Quinones K, Otto-Meyer S. Factors Influencing Short-term Synaptic Plasticity in the Avian Cochlear Nucleus Magnocellularis. J Exp Neurosci 2015; 9:11-24; PMID:26527054; https://doi.org/10.4137/JEN.S25472